



He, E. et al. (2021) SWCNTs/PEDOT:PSS-modified microelectrode arrays for dual-mode detection of electrophysiological signals and dopamine concentration in the striatum under isoflurane anesthesia. *ACS Sensors*, 6(9), pp. 3377-3386. (doi: [10.1021/acssensors.1c01241](https://doi.org/10.1021/acssensors.1c01241))

The material cannot be used for any other purpose without further permission of the publisher and is for private use only.

There may be differences between this version and the published version. You are advised to consult the publisher's version if you wish to cite from it.

<http://eprints.gla.ac.uk/250758/>

Deposited on 13 September 2021

Enlighten – Research publications by members of the University of
Glasgow

<http://eprints.gla.ac.uk>

SWCNTs/PEDOT:PSS-Modified Microelectrode Arrays for Dual-Mode Detection of Electrophysiological Signals and Dopamine Concentration in the Striatum under Isoflurane Anesthesia

Enhui He^{a, b, 1}, Shengwei Xu^{a, b, 1}, Yuchuan Dai^{a, b}, Yiding Wang^{a, b}, Guihua Xiao^{a, b}, Jingyu Xie^{a, b}, Shihong Xu^{a, b}, Penghui Fan^{a, b}, Fan Mo^{a, b}, Mixia Wang^{a, b}, Yilin Song^{a, b}, Huabing Yin^c, Yinghui Li^d, Ying Wang^{e, *} and Xinxia Cai^{a, b, *}

^a State Key Laboratory of Transducer Technology, Aerospace Information Research Institute, Chinese Academy of Sciences, Beijing 100190, China

^b University of Chinese Academy of Sciences, Beijing 100049, China

^c Division of Biomedical Engineering, James Watt School of Engineering, University of Glasgow, Oakfield Avenue, Glasgow, G12 8LT, United Kingdom

^d State Key Laboratory of Space Medicine Fundamentals and Application, China Astronaut Research and Training Center, Beijing 100094, China

^e Department of Anesthesiology, Ruijin Hospital, Shanghai Jiaotong University School of Medicine, 197 Ruijin 2nd Road, Shanghai 200025, China

¹ These authors contributed equally to this work.

* Corresponding Authors

KEYWORDS: *microelectrode array, isoflurane anesthesia, striatum, electrophysiological signal, dopamine, PEDOT, SWCNT*

ABSTRACT: Accurate detection of the degree of isoflurane anesthesia during a surgery is important to avoid the risk of overdose isoflurane anesthesia timely. To address this challenge, a four-shank implantable microelectrode array (MEA) was fabricated for the synchronous real-time detection of dual-mode signals [electrophysiological signal and dopamine (DA) concentration] in rat striatum. The SWCNTs/PEDOT:PSS nanocomposites were modified onto the MEAs, which significantly improved the electrical and electrochemical performances of the MEAs. The electrical performance of the modified MEAs with a low impedance ($16.20 \pm 1.68 \text{ k}\Omega$) and a small phase delay ($-27.76 \pm 0.82^\circ$) enabled the MEAs to detect spike firing with a high signal-to-noise ratio (> 3). The electrochemical performance of the modified MEAs with a low oxidation potential (160 mV), a low detection limit (10 nM), high sensitivity (217 pA/ μM), and a wide linear range (10 nM-72 μM) met the specific requirements for DA detection in vivo. The anesthetic effect of isoflurane was mediated by inhibiting the spike firing of D2_SPNs (spiny projection neurons expressing the D2- type DA receptor) and the broadband oscillation rhythm of the local field potential (LFP). Therefore, the spike firing rate of D2_SPNs and the power of LFP could reflect the degree of isoflurane anesthesia together. During the isoflurane anesthesia-induced death procedure, we found that electrophysiological activities and DA release were strongly inhibited, and changes in the DA concentration provided more details regarding this procedure. The dual-mode recording MEA provided a detection method for the degree of isoflurane anesthesia and a prediction method for fatal overdose isoflurane anesthesia.

Isoflurane is an inhaled general anesthetic with fast onset, stable anesthesia, controllable operation, short anesthesia induction period and recovery period, which has been widely used in animal surgery¹⁻². Many neural signal detection experiments are conducted under isoflurane anesthesia³⁻⁴. However, a large number of studies have shown that isoflurane can change the excitability of brain tissue and cause functional inhibition of brain⁵⁻⁶, and even high concentration of isoflurane can tend to cause death in rats⁷⁻⁸.

Therefore, accurate detection of the degree of isoflurane anesthesia in the surgery is very important.

It is well known that striatum is involved in the process of isoflurane anesthesia⁹⁻¹⁰. Studies have shown that isoflurane can hyperpolarize resting potentials of the neurons of the striatum through the two main anesthetic receptors (gamma-amino butyric acid (GABA) and N-methyl-D-aspartate (NMDA) receptors) in the striatum¹¹⁻¹³, thereby

inhibiting the electrophysiological signals in the striatum¹⁴⁻¹⁵. At the same time, isoflurane can induce biphasic effect on dopamine (DA) regulation by potentiating DA release and inhibiting of DA synthesis in rat striatum¹⁶⁻¹⁷. It is widely accepted that DA plays an important role in anesthesia, and the selective activation of dopaminergic neurotransmission is sufficient to induce emergence from isoflurane general anesthesia^{14,18}. Therefore, the electrophysiological signals and DA concentration in the striatum are both effective indicators to reflect the degree of isoflurane anesthesia.

However, the existing researches are dedicated to studying the effect of isoflurane on single-mode signals (electrophysiological signals or DA)¹⁹⁻²⁰, while isoflurane affects the striatum by simultaneously acting on electrophysiology and DA⁸. Therefore, it is meaningful for the real-time synchronous detection of dual-mode signals (electrophysiological signal and DA concentration) at the cellular level during isoflurane anesthesia process, and even isoflurane anesthesia-induced death procedure^{10,17}. This will help to study the dynamic process of isoflurane anesthesia in more detail, thereby developing a detection method for degree of isoflurane anesthesia and a prediction method for fatal overdose isoflurane anesthesia in the surgery.

At present, electrophysiological signals are commonly recorded by glass micropipettes²¹ or metal wire electrodes²² that can be fabricated simply but offer imprecise spacing and size. And the isoflurane-induced DA are detected using microdialysis method which is high sensitivity and selectivity but poor spatial and temporal resolution according to the previous studies^{16,21,23}. The above methods focus on

single-mode signals such as electrophysiological signal or DA release²⁴⁻²⁵. To detect the dynamic variations of striatal dual-mode signals during isoflurane anesthesia in real time, a highly sensitive, highly selective, and high-temporal resolution implantable microelectrode array (MEA) that can simultaneously detect electrophysiological signals and DA concentrations is needed²⁶⁻²⁸.

At the same time, to improve the detection ability of MEA, the nanomaterials are modified onto the surface of MEA²⁹. In recent years, poly (3,4-ethylenedioxythiophene) polystyrene sulfonate (PEDOT:PSS) has been widely used in MEA to detect electrophysiological signals and neurotransmitters owing to good adhesion and porous structure³⁰⁻³². In addition, carbon nanotubes (CNTs) were embedded into PEDOT to enhance conductivity, biocompatibility and stability of the MEA owing to their extraordinary strength, electrical conductivity and chemical stability³²⁻³⁴.

In our work, a dual-mode recording MEA was mass fabricated for synchronous real-time detection of electrophysiological signals and DA concentrations in rat striatum. In addition, the SWCNTs/PEDOT:PSS nanocomposites were modified onto the MEA to improve their electrical performance and electrochemical performance. The MEAs were implanted into the rat striatum to detect dual-mode signals. The *in vivo* studies demonstrated that the modified MEA could stably and sensitively record the electrophysiological signals and DA concentrations in rat striatum. And the characters of dynamic variations of dual-mode signals provided a detection method for degree of isoflurane anesthesia and a prediction method for fatal overdose isoflurane anesthesia.

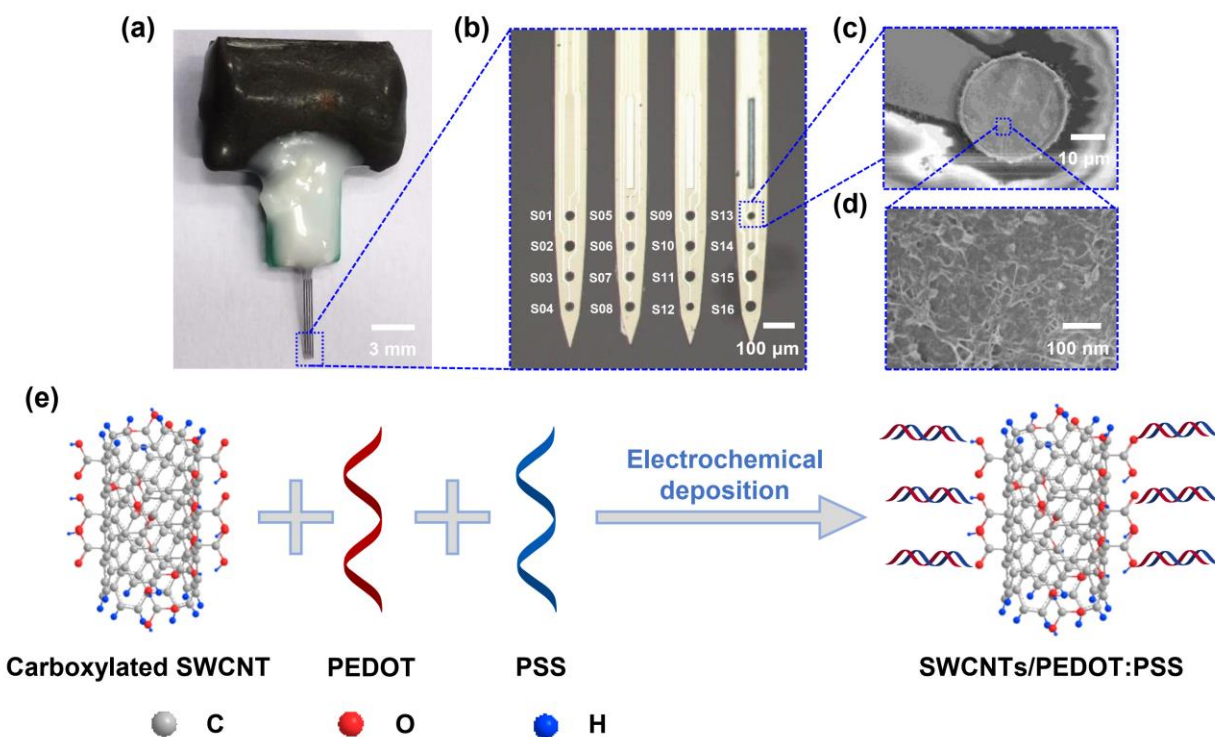


Figure 1. SWCNTs/PEDOT:PSS modified microelectrode arrays. (a) The completed MEA connected with the printed circuit board. (b) 16 microelectrodes are distributed on the tip of four shanks. (c) Morphology of the SWCNTs/PEDOT:PSS modified microelectrode characterized by scanning electron microscopy (SEM). (d) SEM image of the SWCNTs/PEDOT:PSS nanocomposites. (e) Scheme for electrochemical deposition of SWCNTs/PEDOT:PSS onto the microelectrodes.

The MEA was designed with 16 microelectrodes. Each microelectrode could detect either electrophysiological signals or dopamine concentration, depending on whether the microelectrode is connected to an electrophysiological module or an electrochemical module (Figure 1a). As shown in Figure 1b, the implantable part of the MEA was designed with four shanks (6 mm long; 100 μm wide; 30 μm thick). Each shank contained 4 microelectrodes (20 μm electrode diameter and 100 μm spacing). The MEA was mass fabricated by Micro-Electro-Mechanical System (MEMS) technique as previously described³⁵. The details of the fabrication process are shown in the supporting information.

SWCNTs/PEDOT:PSS nanocomposites for dual-mode recording

In order to simultaneously detect the electrophysiological signals and DA concentration of rat striatum in real time, all microelectrodes (S01~S16) were modified with SWCNTs/PEDOT:PSS nanocomposites as following steps: Firstly, 165.88 mg PSS and 10 ml carboxylic ultrapure single-wall carbon nanotubes (SWCNTs) aqueous dispersion (0.15 wt%) were mixed by ultrasonically dispersed for at least 30 min. Secondly, 22.74 mg EDOT was mixed into the dispersed solution, followed by 30 min ultrasonic dispersion. Then, the deposition was performed in the dispersed solution by cyclic voltammetry (CV) between 0 and 0.95 V at a rate of 100 mV/s for 20 cycles using an Ag|AgCl (sat. KCl) reference electrode and a Pt counter electrode. The

scheme for electrochemical deposition of the nanocomposite is shown in Figure 1e.

Dual-mode recording MEA Characterization and Testing

To characterize the electrical performance of the MEA, all microelectrodes underwent electrochemical impedance spectroscopy (EIS) in standard PBS (± 10 mV vs Ag|AgCl, 100 kHz - 10 Hz). To characterize the electrochemical performance of MEA for detecting DA, all microelectrodes were tested in vitro with the homemade dual-mode recording equipment based on traditional three-electrode system. The test methods included cyclic voltammetry (CV) and amperometry.

In vivo dual-mode recording under isoflurane anesthesia

As shown in Figure S1, the whole experiment comprises an anesthesia machine, a mask, a modified MEA and a homemade dual-mode recording equipment (design details are shown in supporting information). Sprague-Dawley (SD) rats were anesthetized with the different concentration of isoflurane (1.5% \rightarrow 1.0% \rightarrow 0.5%). The dual-mode signals, including electrophysiological signals (neural spike signals and local field potentials (LFPs)) and DA concentration, in rat striatum were recorded by the MEA. The implantation position of the MEA is shown in Figure S2.

In addition, the details of surgery, experiment, MEA recording, signal processing and analysis are presented in the supporting information.

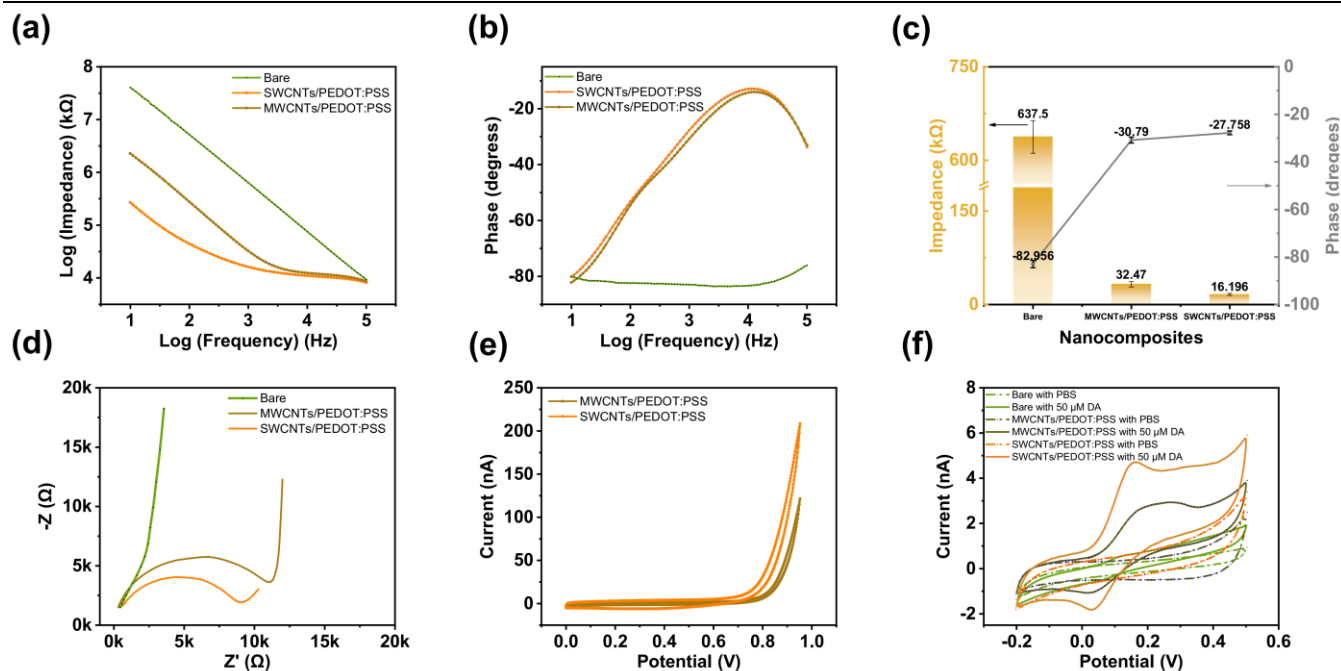


Figure 2. Electrical (a-d) and electrochemical (e, f) performance characterization of the MEA. (a) Impedance characteristics of bare and modified microelectrodes at different frequencies. (b) Phase characteristics of bare and modified microelectrodes at different frequencies. (c) At 1 kHz frequency, the impedance and phase of the bare microelectrodes, MWCNTs/PEDOT:PSS modified microelectrodes and SWCNTs/PEDOT:PSS modified microelectrodes. (d) Nyquist plots of the complex plane impedance spectra of bare and modified microelectrodes. (e) Cyclic voltammograms of MWCNTs/PEDOT:PSS and SWCNTs/PEDOT:PSS deposition process. (f) Cyclic voltammograms of the bare microelectrodes, MWCNTs/PEDOT:PSS modified microelectrodes and SWCNTs/PEDOT:PSS modified microelectrodes in 50 μM DA and PBS, respectively (-0.2 - 0.5 V, 100 mV/s, 5 cycles). (n = 5).

RESULTS AND DISCUSSION

Electrical performance characterization of the MEA

As shown in Figure 1c,d, the SEM images indicate that the SWCNTs/PEDOT:PSS nanocomposites are tightly adhere to the surface of the microelectrodes. The nanocomposites form many nanostructures and provide a rougher and po-

rous surface, which is conducive to improving the conductivity of the microelectrodes.

As shown in Figure 2a,b, the impedance and the phase of the bare microelectrodes and the modified microelectrodes are compared in the frequency range from 10 Hz to 100 kHz. At 1 kHz frequency (central frequency of the neural activity), the impedance of the microelectrodes decreases from $637.5 \pm 26.24 \text{ k}\Omega$ (bare) to $32.47 \pm 4.22 \text{ k}\Omega$ (MWCNTs/PEDOT:PSS), and then to $16.20 \pm 1.68 \text{ k}\Omega$ (SWCNTs/PEDOT:PSS) ($n = 5$, $***p < 0.001$). The phases of the microelectrodes increase from $-82.95 \pm 1.54^\circ$ (bare) to $-30.79 \pm 1.27^\circ$ (MWCNTs/PEDOT:PSS), and then to $-27.76 \pm 0.82^\circ$ (SWCNTs/PEDOT:PSS) ($n = 5$, $***p < 0.001$) (Figure 2c). As shown in Figure S3, the active surface areas of the microelectrodes were evaluated using double layer capacitance (C_{dl}) from cyclic voltammetry experiments, and the results indicated that the SWCNTs/PEDOT:PSS modified microelectrodes ($C_{dl} = 0.852 \text{ nF}$) had larger active surface areas and more active sites than MWCNTs/PEDOT:PSS modified microelectrodes ($C_{dl} = 0.296 \text{ nF}$) (details in "Comparison of active surface area of SWCNTs/PEDOT:PSS and MWCNTs/PEDOT:PSS modified microelectrodes" of supporting information). The above results mean that the SWCNTs/PEDOT:PSS modified microelectrodes have the best electrical performance with the lowest impedance and the smallest phase delay, because of the larger active surface area and more active sites. At the same time, the phases of the SWCNTs/PEDOT:PSS and MWCNTs/PEDOT:PSS modified microelectrodes are similar, which indicates that the reduction in phase delay is mainly attributed to the PEDOT. Furthermore, Nyquist plots of the impedance spectra of the bare and modified microelectrodes further demonstrate that SWCNTs/PEDOT:PSS modified microelectrodes have strong indication of diffusional characteristics (Figure 2d).

Electrochemical performance characterization of the MEA

During the growth of SWCNTs/PEDOT:PSS and MWCNTs/PEDOT:PSS nanocomposite films, the recorded cyclic voltammograms are the typical characteristic for PEDOT polymerization (Figure 2e). Under the same electrochemical deposition condition, the deposition current of SWCNTs/PEDOT:PSS nanocomposites is larger than that of MWCNTs/PEDOT:PSS nanocomposites.

To obtain the current responses of the bare and the modified microelectrodes to the DA solution, CV was applied to the bare and the modified microelectrodes in PBS and $50 \mu\text{M}$ DA solution, respectively. As shown in Figure 2f, compared to the bare microelectrodes, modified sites have obvious current responses to the DA solution. The oxidation peak potential is 160 mV for SWCNTs/PEDOT:PSS modified microelectrodes and 250 mV for MWCNTs/PEDOT:PSS modified microelectrodes, whereas the bare microelectrodes have no obvious oxidation peak potential as well as the weak current response to DA. The results indicate that the nanocomposites modified microelectrodes can catalyze the DA reaction. Furthermore, the oxidation potential of SWCNTs/PEDOT:PSS modified microelectrodes to DA is much lower than that of MWCNTs/PEDOT:PSS modified microelectrodes, and the oxidation current of SWCNTs/PEDOT:PSS modified microelectrodes to DA is much more larger than that of MWCNTs/PEDOT:PSS modified microelectrodes. A lower DA oxidation potential is important for the safety of in vivo detection and is vital to avoid various interfering reactions.

The calibration was performed under a three-electrode system in a PBS solution. The chronoamperometry was applied with the potential of 160 mV for SWCNTs/PEDOT:PSS modified microelectrodes and 250 mV for MWCNTs/PEDOT:PSS modified microelectrodes. Figure 3a shows typical low concentration calibration curves of SWCNTs/PEDOT:PSS and MWCNTs/PEDOT:PSS within a concentration range from 10 nM to 500 nM . Figure 3b shows typical calibration curves of SWCNTs/PEDOT:PSS (500 nM to $72 \mu\text{M}$) and MWCNTs/PEDOT:PSS ($1 \mu\text{M}$ to $59 \mu\text{M}$). In low concentration, SWCNTs/PEDOT:PSS nanocomposites have obvious current responses to DA, while MWCNTs/PEDOT:PSS nanocomposites have no obvious current response. As shown in Figure 3c, the DA concentration and the current responses are piecewise linear for SWCNTs/PEDOT:PSS nanocomposites, that is, in the range from 10 nM to $4 \mu\text{M}$, the linear equation is $I \text{ (pA)} = 217C \text{ (}\mu\text{M)} + 134$, with a correlation coefficient of 0.9816 , and in the range from $4 \mu\text{M}$ to $72 \mu\text{M}$, the linear equation is $I \text{ (pA)} = 42C \text{ (}\mu\text{M)} + 1071$, with a correlation coefficient of 0.9717 . The sensitivities are $217 \text{ pA}/\mu\text{M}$ and $42 \text{ pA}/\mu\text{M}$, respectively. The MWCNTs/PEDOT:PSS nanocomposites have a linear current response within a DA concentration range from $1 \mu\text{M}$ to $59 \mu\text{M}$, whose sensitivity is $19.6 \text{ pA}/\mu\text{M}$.

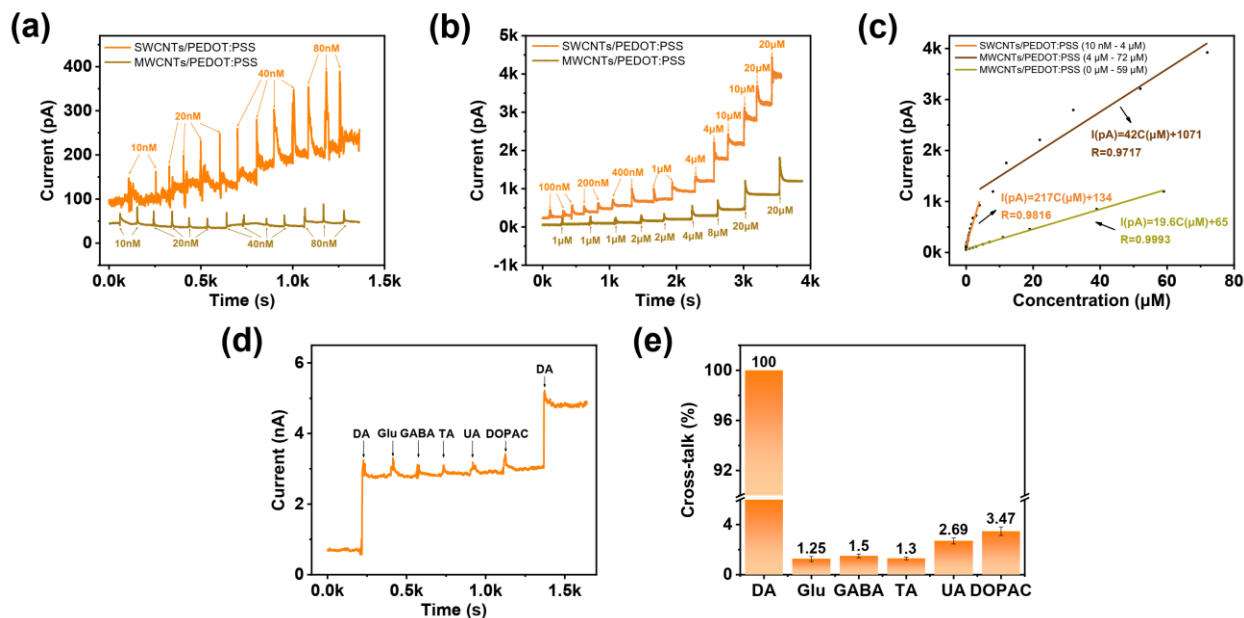


Figure 3. Electrochemical performance characterization of the MEA. (a) Typical low concentration calibration curves of SWCNTs/PEDOT:PSS and MWCNTs/PEDOT:PSS within a concentration range from 10 nM to 500 nM. (b) Typical calibration curves of SWCNTs/PEDOT:PSS (500 nM to 72 μM) and MWCNTs/PEDOT:PSS (1 μM to 59 μM). (c) Piecewise linear fitting curves of DA current responses for SWCNTs/PEDOT:PSS in the concentration range from 10 nM to 4 μM and 4 μM to 72 μM , respectively. And the linear fitting curve of DA current response for MWCNTs/PEDOT:PSS in the concentration range from 1 μM to 50 μM . (d) SWCNTs/PEDOT:PSS nanocomposites current responses to the addition of interferers (Glu, GABA, TA, UA and DOPAC) with a concentration of 50 μM . (e) Current response comparison between the interferers and DA ($n = 5$).

Table.1 The electrochemical performance parameters of SWCNTs/PEDOT:PSS and MWCNTs/PEDOT:PSS nanocomposites.

Nanocomposites	Oxidation potential [mV]	Detection limit [nM]	Linear range [μM]	Sensitivity [$\text{pA}/\mu\text{M}$]	R
MWCNTs/PEDOT:PSS	250	1000	1-59	19.6	0.9993
SWCNTs/PEDOT:PSS	160	10	0.01-4 4-72	217 42	0.9816 0.9717

The electrochemical performance parameters of SWCNTs/PEDOT:PSS and MWCNTs/PEDOT:PSS are compared in Table 1. The results show that SWCNTs/PEDOT:PSS nanocomposites have lower oxidation potential, lower detection limit, higher sensitivity and larger linear range than MWCNTs/PEDOT:PSS nanocomposites. Therefore, compared to MWCNTs/PEDOT:PSS nanocomposites, SWCNTs/PEDOT:PSS nanocomposites have better electrochemical performance, which is conducive to the detection of trace DA in vivo.

To verify the selectivity of the SWCNTs/PEDOT:PSS nanocomposites, common interferers, including Glutamate (Glu), γ -aminobutyric acid (GABA), Taurine (TA), Uric acid (UA) and 3,4-Dihydroxyphenylacetic acid (DOPAC) were added into the 50 μM DA solution (reaction potential

was 160 mV) (Figure 3d). As shown in Figure 3e, the calculated selectivity ratio for DA to Glu, GABA, TA, UA and DOPAC (concentration is all 50 μM) is 1.25%, 1.5%, 1.3%, 2.69%, 3.47%, respectively, which satisfied the requirement of the in vivo detection.

To evaluate the stability of SWCNTs/PEDOT:PSS nanocomposites on microelectrodes, the morphology, the impedances and the phases of the SWCNTs/PEDOT:PSS modified microelectrodes were compared before and after implantation. As shown in Figure S4, the SWCNTs/PEDOT:PSS nanocomposites on microelectrodes are stable before and after implantation, and the nanocomposites will not detach from the microelectrodes (details in "The stability of SWCNTs/PEDOT:PSS nanocomposites on microelectrodes" of supporting information).

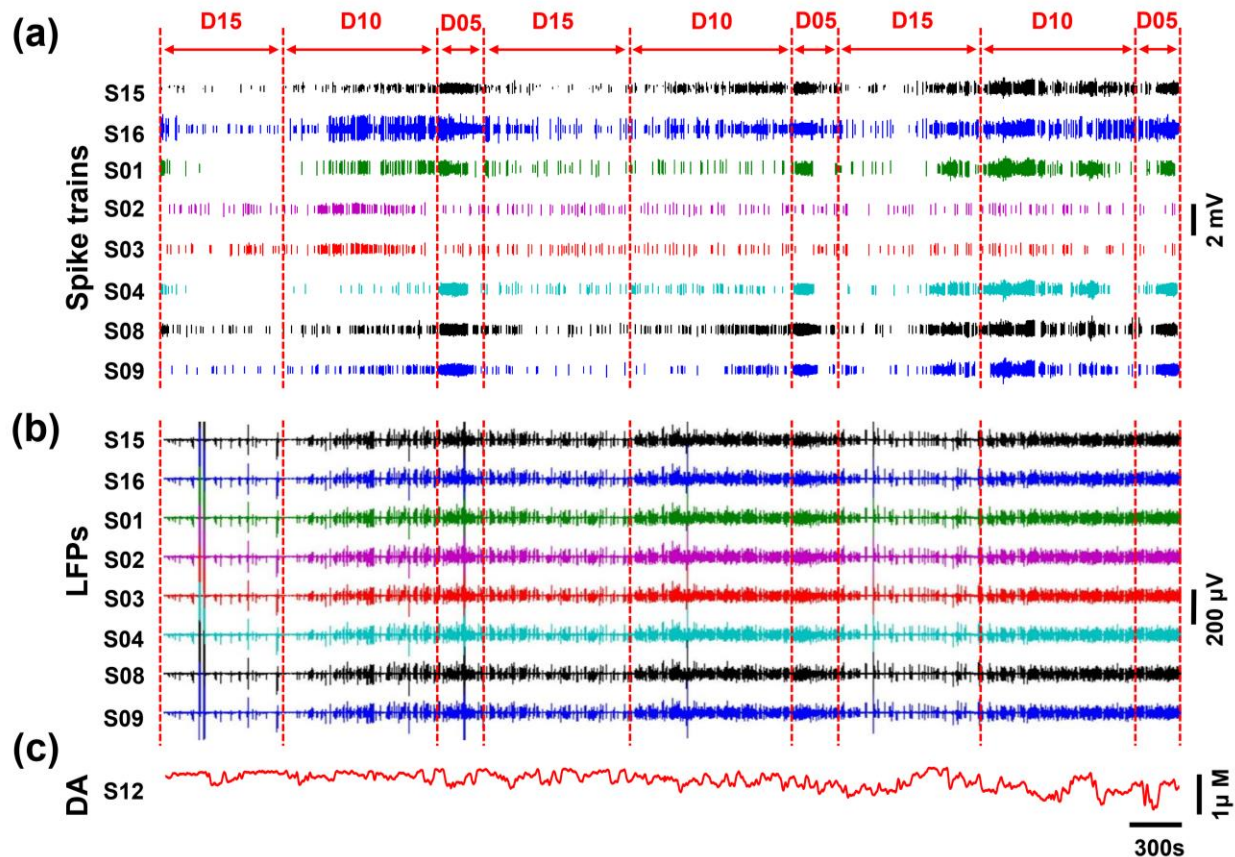


Figure 4. Dynamic variations of the dual-mode signals of isoflurane anesthetic procedure. D15, D10 and D05 represent that the rat was anesthetized with 1.5%, 1.0% and 0.5% isoflurane, respectively. (a) Representative eight channels of spike trains and (b) LFPs recorded by the MEA. They were modulated by the concentration of isoflurane obviously. (c) Representative channel of DA concentration recorded by the MEA.

Dynamic variations of the dual-mode signals of isoflurane anesthetic procedure

Figure 4 shows that the typical dynamic variations of neural electrophysiological signals (neural spike signals and LFPs) and DA concentration which were recorded in the striatum throughout a typical anesthetic procedure. The D15, D10 and D05 represented that the rat was anesthetized with 1.5%, 1.0% and 0.5% isoflurane, respectively. In terms of neural electrophysiological signal, the spikes and LFPs detected by eight representative sites exhibited a regular change with the concentration of isoflurane. As shown in Figure 4a,b and Figure S5, in the three anesthesia cycles, the spike firing activities and LFPs had typical pattern in the three concentration of D15, D10 and D05. In the D15, the neural spike firing was in silent-firing pattern, and the fluctuation and amplitude of LFPs were small. When in the D10, the neural spike firing entered tonic-firing pattern, and the fluctuation and amplitude of LFPs increased. After entering the D05, the neural spike firing entered burst-firing pattern, and the fluctuation and amplitude of LFPs enhanced rapidly. At the same time, the rat breathed quickly and was about to wake up. When the rat was anesthetized with 1.5% isoflurane again, the patterns of neural spike firing and LFPs could return to the stage of D15 quickly. In terms of electrochemical signal, the DA concentration was relatively stable and did not show a regular change as concentration of isoflurane (Figure 4c).

The recorded results show the detailed dynamic process of isoflurane anesthesia. It can be seen that the spike firing activities and the fluctuation of LFPs significantly increase

as the degree of isoflurane anesthesia decreases. In different concentration of isoflurane, neural spike firing and LFPs change simultaneously, and their responses to the degree of isoflurane anesthesia are repeatable and reversible. This means that they can be used to define the degree of isoflurane anesthesia together.

Characteristics of the dual-mode signals at different degrees of isoflurane anesthesia

In the striatum, spiny projection neurons (SPNs) account for 95% of the neurons³⁶. SPNs are usually divided into two types of neurons which express the D1-type DA receptor (D1_SPNs) and the D2-type DA receptor (D2_SPNs)³⁶⁻³⁷. D1_SPNs and D2_SPNs differ with respect to both synaptic inputs and projection targets³⁷.

Therefore, according to the reported methods³⁸⁻⁴⁰, the recorded spikes were classified by the following methods: First, offline sorting was performed for recorded spikes to obtain single neuron signals (spike unit) via principal component analysis (PCA) and valley seeking methods. Then, the spike duration and symmetry index of all 44 separate spike units were calculated. Finally, all units were classified into two types (25 D1_SPNs and 19 D2_SPNs) by K-means cluster analysis (Figure 5a). Figure S6 show the statistical analysis of the spike duration and symmetry index of D1_SPNs and D2_SPNs. The aggregated waveforms in Figure 5b show that the waveform of D1_SPN is higher and narrower than that of the D2_SPN. The spike firing rates of D1_SPNs and D2_SPNs at different degrees of isoflurane anesthesia were statistically analyzed respec-

tively. As shown in Figure 5c, the spike firing rates of D1_SPNs and D2_SPNs all increase with the degree of isoflurane anesthesia decreases. Furthermore, the spike firing rates of D2_SPNs are significantly different between the three degrees of isoflurane anesthesia ($n = 19$; $***P <$

0.001), while the change of spike firing rates of D1_SPNs is not obvious enough ($n = 25$; $*P < 0.05$). Indicate that the response of D2_SPNs to the different degree of isoflurane anesthesia is more obvious than that of D1_SPNs.

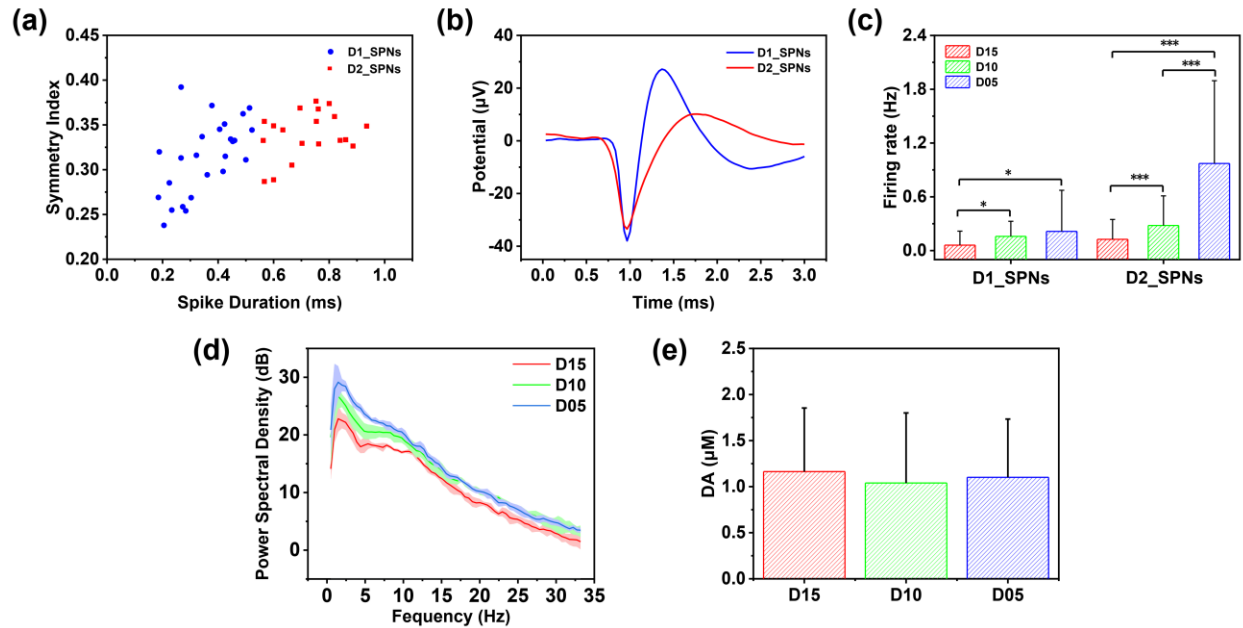


Figure 5. Characteristics of the dual-mode signals at different degrees of isoflurane anesthesia. (a) All 44 separate spike units were classified into 25 D1_SPNs and 19 D2_SPNs by K-means clustering with the parameters of spike duration and symmetry index. (b) The aggregated waveforms of D1_SPNs and D2_SPNs. (c) Statistical analysis of the average spike firing rates of D1_SPNs and D2_SPNs at the different degrees of isoflurane anesthesia. (d) The PSD of LFPs in the frequency band of 0-33 Hz. The shadow is the error bar calculated from the PSD of the LFPs recorded by 8 channels. (e) Statistical analysis of the DA concentration at the different degrees of isoflurane anesthesia. ($n = 8$; $*P < 0.05$; $**P < 0.01$; $***P < 0.001$).

LFP is a complex combination of electrophysiological activities of a group of neurons surrounding the microelectrodes⁴¹. Figure S7a depicts the power density spectrogram of LFPs in the frequency (0-33 Hz) during the whole anesthetic procedure. As shown in Figure 5d, the PSD of LFPs significantly increase as the degree of isoflurane anesthesia decreases, which is highly consistent with the PSD of D2_SPN spikes (Figure S7b). Indicate that the electrophysiological signals of the cell level and the population cell level are consistent in response to isoflurane anesthesia. Furthermore, the power spectral densities (PSD) of LFPs indicate that the frequency components of LFPs are mainly distributed in the 0-14 Hz. Therefore, the power of the delta rhythm (1-3 Hz), theta rhythm (4-7 Hz) and alpha rhythm (8-14 Hz) bands of the LFPs are statistically analyzed at each degree of isoflurane anesthesia respectively (Figure S7c). The results show that at the different degrees of isoflurane anesthesia, the power of LFP is significantly different in the whole and different frequency bands, and the power of LFPs increases with the degree of isoflurane anesthesia decreases.

As shown in Figure 6e, DA concentration are statistically analyzed at the different degree of isoflurane anesthesia. The average DA concentration in the stages of D15, D10 and D05 are $1.163 \pm 0.690 \mu\text{M}$, $1.040 \pm 0.761 \mu\text{M}$ and $1.101 \pm 0.633 \mu\text{M}$, respectively, which have no significant difference.

Quantitative analysis of spike and LFPs show that isoflurane does inhibit the electrophysiological activities of the striatum. According to the previous studies, isoflurane inhibits the neural activities by targeting GABA and NMDA

receptors which were distributed in the striatum¹¹⁻¹⁵. Our results further indicate that as a general anesthetic, isoflurane not only inhibit the spike firing at the cellular level, but also inhibit the neuronal population activities by suppressing the oscillation rhythm over a wide spectrum band of the LFP. At the same time, the D2_SPNs are more obviously regulated by the isoflurane anesthesia than D1_SPNs. The reason may be that D2_SPNs displayed a larger ratio of NMDA receptor mediated excitatory postsynaptic currents, which make D2_SPNs more excitable⁴². We infer that the anesthetic effect of isoflurane in the striatum maybe mainly caused by the inhibition of D2_SPNs.

Some studies based on in vivo microdialysis techniques showed that isoflurane anesthesia could induce biphasic effect on DA regulation by potentiating DA release and inhibiting of DA synthesis in rat striatum¹⁶⁻¹⁷. The in vivo fast scan cyclic voltammetry (FSCV) techniques indicated that surgical level isoflurane concentration would not significantly alter terminal mechanisms of DA release and uptake^{20, 43}. Our results also confirm the above conclusions and further find that under surgical level isoflurane concentration, the DA concentration will fluctuate during anesthesia procedure, but the average DA concentration is not significantly different with the degree of isoflurane anesthesia.

In summary, there is an excellent negative correlation between the degree of isoflurane anesthesia and the spike firing rate of D2_SPNs and the power of LFP, which means the two electrophysiological indexes can reflect the degree of isoflurane anesthesia in real time. This provides a detection method for degree of isoflurane anesthesia.

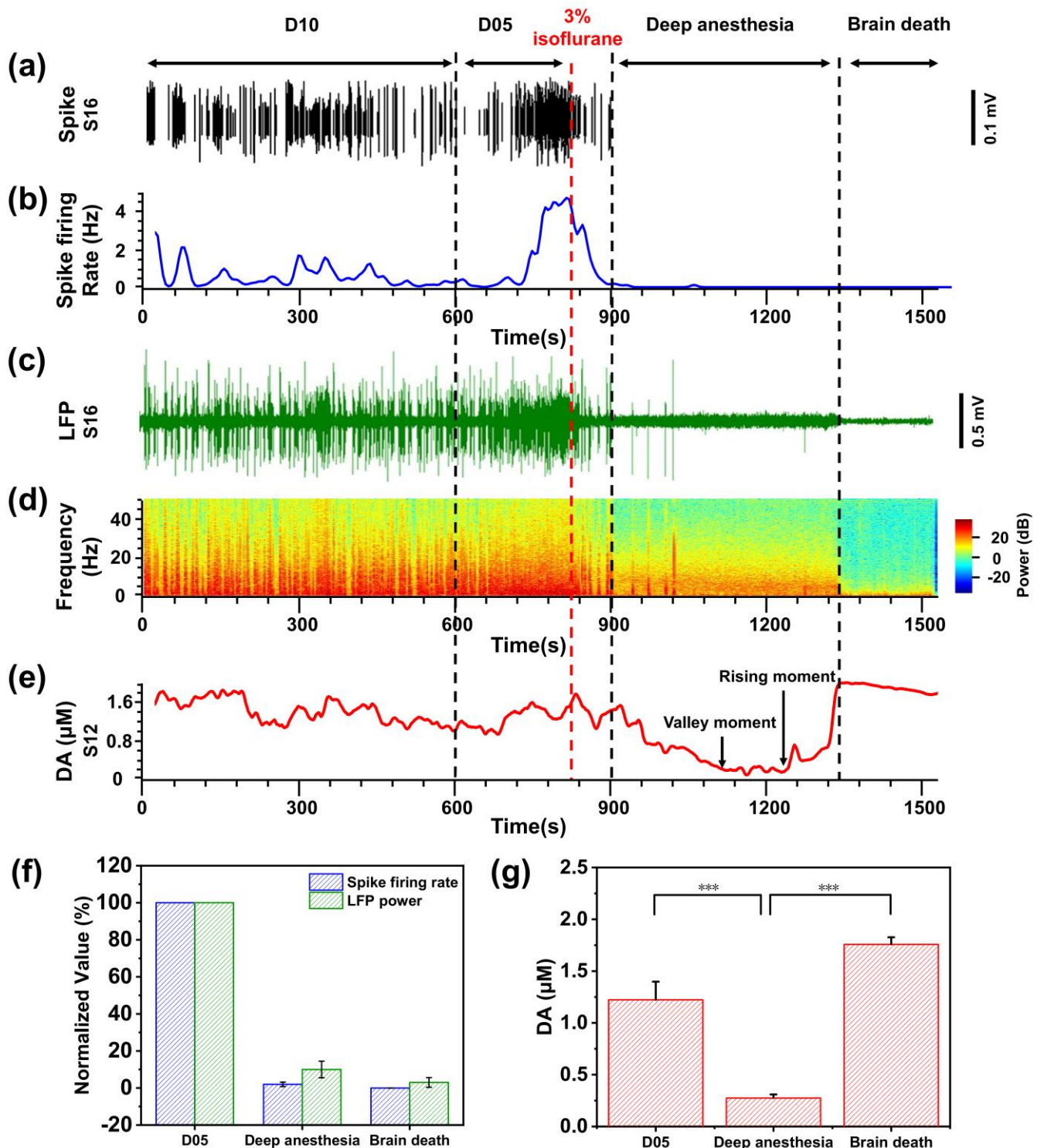


Figure 6. Characteristics of the dual-mode signals during isoflurane anesthesia-induced death procedure. (a) The spike firing of D2_SPNs was recorded by S16. (b) The average spike firing rate histogram of D2_SPNs (n = 8). (c) The LFP was recorded by S16. (d) The spectrogram of LFPs (n = 8). (e) The DA concentration was recorded by S12. “Valley moment” and “Rising moment” represent the moment when the DA concentration drops to the bottom and rises from the bottom, respectively. (f) Statistical analysis of spike firing rate and LFP power at the stages of D05, deep anesthesia and brain death. All data points are normalized to the average values of the D05 (n = 3). (g) Statistical analysis of DA concentration at the stages of D05, deep anesthesia and brain death (n = 3; ***P < 0.001).

Characteristics of the dual-mode signals during isoflurane anesthesia-induced death procedure

The characteristics of the dual-mode signals during isoflurane anesthesia-induced death procedure were analyzed. Figure 6a,c,e show the electrophysiology signal of a repre-

sentative channel (S16) and the electrochemical signal of DA concentration of a representative channel (S12) when the isoflurane concentration increased from 0.5% to 3%. The dual-mode signals of other channels were similar. According to the above result that the D2_SPNs were more obviously regulated by the degrees of isoflurane anesthe-

sia than D1_SPNs, we selected D2_SPNs as the analysis object of neural spike firing. As shown in Figure 6a-d, when the rat was anesthetized with 3% isoflurane, the spike firing rate rapidly decreased, the fluctuation of the LFP became smaller quickly, and the power of the frequency components of the LFPs were significantly reduced. After about 70 s, the spikes firing and the wide fluctuation of the LFP were almost disappeared, and the rat brain entered a state of deep anesthesia. The state of deep anesthesia was maintained for about 470 s. Then, the fluctuation of the LFP dropped to close to zero suddenly, and its frequency components almost completely disappeared. At that time, the rat had stopped breathing. According to the definition of brain death⁴⁴⁻⁴⁵, it could be determined that the rat brain was dead. The statistical analysis showed that compared the stage of D05, the average spike firing rate dropped to $2 \pm 1\%$ (deep anesthesia), and then dropped to 0% (brain death). The average LFP power dropped to $10 \pm 5\%$ (deep anesthesia), and then dropped to $3 \pm 2\%$ (brain death), as shown in Figure 6f.

In the terms of DA concentration, as described above, when under surgical level isoflurane concentration, the DA concentration fluctuates within a certain range, which is not significantly related to the degrees of isoflurane anesthesia. However, when the rat was anesthetized with 3% isoflurane, the DA concentration decreased significantly (Figure 6e). After about 300 s, the DA concentration dropped to the bottom, and maintained in the bottom for about 140 s. Then, it began to rise for 100 s and reached the peak when the rat brain died. Thereafter, due to the consumption of electrochemical measurement, the DA concentration slowly decreased without fluctuation, which further confirmed that the brain had been dead. Further statistical analysis showed that the average DA concentration dropped from $1.22 \pm 0.18 \mu\text{M}$ (D05) to $0.27 \pm 0.04 \mu\text{M}$ (deep anesthesia), and then rose to $1.76 \pm 0.07 \mu\text{M}$ (brain death), as shown in Figure 6g.

There are growing evidence that overdose isoflurane may cause widespread apoptosis of neurons, and even induce brain death, in the rodents and nonhuman primates⁴⁶⁻⁴⁸. Our results showed that during the isoflurane anesthesia-induced death procedure, the neural electrophysiology activities changed faster and suddenly, while the change of the DA concentration was relatively slower and smoother. Overdose isoflurane anesthesia would inhibit electrophysiology activities quickly. After entering the state of deep anesthesia, the electrophysiology activities no longer changed, while the change of the DA concentration provided more details for the isoflurane anesthesia-induced death procedure. A possible understanding of the isoflurane anesthesia-induced death procedure was that, at the "Valley moment" when the DA concentration dropped to the bottom, neurons no longer released DA, and the normal function of the brain was inhibited completely which make the brain in dangerous. At the "Rising moment", when the DA concentration rose from the bottom, neurons began to release DA abnormally, and the brain had started the death procedure. Finally, at the moment of "Brain death", DA was no longer released, and the brain had been dead.

Due to individual differences, even the surgical level isoflurane concentration may be excessive for some rats, which easily causes the death. In addition, the isoflurane anesthesia-induced death usually happens suddenly, which makes it difficult to predict. Therefore, it is important to accurately detect the degree of isoflurane anesthesia, especially predict the fatal overdose isoflurane anesthesia in the surgery.

The above results prove that the dual-mode signals especially the DA concentration, can provide the dynamic process of isoflurane anesthesia-induced death procedure in more detail. Therefore, as shown in Table S2, the quantitative dual-mode signals can predict the four stages of anesthesia-induced death procedure: Shallow Anesthesia - Overdose Anesthesia - Deep Anesthesia (I, II, III) - Brain Death. The details of the prediction method for fatal overdose isoflurane anesthesia are presented in the supporting information. Simply, if the electrophysiology activities are inhibited rapidly accompanied by a decrease of DA concentration in the rat striatum, the degree of isoflurane anesthesia has reached deep anesthesia which is sufficient to induce death. The deep anesthesia will last for some time. When the DA concentration begin to rise, it indicates that the brain may begin to die.

In summary, the dual-mode signals provide a prediction method of whether the degree of isoflurane anesthesia is sufficient to induce death. During the surgery, the real-time detection of dual-mode signals can avoid the risks of overdose isoflurane anesthesia timely.

CONCLUSION

In this work, we designed and fabricated a four-shank implantable MEA which was used to simultaneously detect the dual-mode signals (electrophysiological signal and DA concentration) in the striatum during isoflurane anesthesia process and isoflurane anesthesia-induced death procedure. To improve the performance of the MEA, the SWCNTs/PEDOT:PSS nanocomposites were modified onto the MEA. The SWCNTs/PEDOT:PSS modified MEA has the better electrical performance and electrochemical performance. The better electrical performances allow the MEA to detect electrophysiological signals with a high signal-to-noise ratio (SNR). The better electrochemical performances allow the MEA have the sensitive and selective respond to DA concentration. The dual-mode signals recorded by the MEA show the spike firing rate of D2_SPNs and the power of LFP can reflect the degree of isoflurane anesthesia accurately. The electrophysiological signals and DA concentration can jointly reflect the isoflurane anesthesia-induced death procedure.

Compared to the reported works of CNTs/PEDOT:PSS modified MEAs in Table S1, the novelty of our work include the following three points: (1) detailed comparison and characterization of SWCNTs/PEDOT:PSS and MWCNTs/PEDOT:PSS; (2) the CNTs/PEDOT:PSS modified MEA was applied to simultaneously detect dual-mode signals of electrophysiological signals and DA concentration for the first time; (3) revealing the interact of electrophysiology and DA electrochemical signals under isoflurane anesthesia for the first time.

The use of dual-mode recording MEA allow us to study the dynamic process of isoflurane anesthesia in detail. The characters of the dual-mode signals recorded by MEA provide a detection method for degree of isoflurane anesthesia and a prediction method for fatal overdose isoflurane anesthesia in the surgery. In the further, this method will be used to test the toxicity and lethality of inhaled anesthetics, such as desflurane and sevoflurane which are commonly used in clinical practice. If the dual-mode signals can be correlated with the EEG to find the characteristics of the EEG during isoflurane anesthesia-induced death procedure. This will help to develop a clinical noninvasive technique for monitoring anesthesia-induced death, which is important for reducing the risk of anesthesia in clinic.

AUTHOR INFORMATION

Supporting Information

Materials and methods, recording equipment , implantation position of the MEA, experimental procedure, comparison of the active surface area and stability of SWCNTs/PEDOT:PSS nanocomposites, comparison of typical electrophysiology patterns, comparison of the characteristics between D1_SPNs and D2_SPNs, characteristics of the LFPs at different degrees of isoflurane anesthesia, comparison of CNTs/PEDOT:PSS-modified MEAs, and the dynamic process of the quantitative dual-mode signal of isoflurane-induced death procedure (PDF)

Corresponding Author

Email: xxcai@mail.ie.ac.cn (Xinxia Cai)

wy10879@rjh.com.cn (Ying Wang)

Author Contributions

Enhui He Shengwei Xu contributed equally to this work. E. He, S. Xu, Y. Wang and X. Cai designed the research plan and experiments. E. He and S. Xu wrote the manuscript. S. Xu, Y. Dai, G. Xiao and Y. Wang fabricated the MEA. E. He and S. Xu conducted the experiments and analyzed the experimental data. Y. Dai, G. Xiao, Y. Wang, J. Xie, S. Xu, P. Fan, Y. Song provided the experimental help. G. Xiao, F. Mo, M. Wang, Y. Song, H. Yin and Y. Li provided help in results analysis. All the authors read and approved the final manuscript.

Notes

The authors declare no competing financial interest.

ACKNOWLEDGMENT

This work was sponsored by the National Natural Science Foundation of China (Nos. 61960206012, 62121003, 61971400, 61771452, 61775216, 61975206, and 61973292), the Scientific Instrument Developing Project of the Chinese Academy of Sciences (No. GJJSTD20210004), the National Key Research and Development Program (2017YFA0205902), the Youth Innovation Promotion Association, CAS, and the opening foundation of the State Key Laboratory of Space Medicine Fundamentals and Application, Chinese Astronaut Research and Training Center (No. SMFA19K05).

REFERENCES

1. Eger, E. I., THE PHARMACOLOGY OF ISOFLURANE. *Br. J. Anaesth.* 1984, 56 (1), S71-S99.
2. Shaughnessy, M. R.; Hofmeister, E. H., A systematic review of sevoflurane and isoflurane minimum alveolar concentration in domestic cats. *Vet. Anaesth. Analg.* 2014, 41 (1), 1-13.

3. Dai, Y.; Song, Y.; Xie, J.; Xiao, G.; Li, X.; Li, Z.; Gao, F.; Zhang, Y.; He, E.; Xu, S.; Wang, Y.; Zheng, W.; Jiang, X.; Qi, Z.; Meng, D.; Fan, Z.; Cai, X., CB1-Antibody Modified Liposomes for Targeted Modulation of Epileptiform Activities Synchronously Detected by Microelectrode Arrays. *ACS Appl Mater Interfaces* 2020, 12 (37), 41148-41156.
4. Li, X.; Song, Y.; Xiao, G.; Xie, J.; Dai, Y.; Xing, Y.; He, E.; Wang, Y.; Xu, S.; Zhang, L., Flexible Electro-corticography Electrode Array for Epileptiform Electrical Activity Recording under Glutamate and GABA Modulation on the Primary Somatosensory Cortex of Rats. *Micromachines* 2020, 11 (8), 732.
5. PurteLL, K.; Gingrich, K. J.; Ouyang, W.; Herold, K. F.; Hemmings, H. C., Activity-dependent depression of neuronal sodium channels by the general anaesthetic isoflurane. *Br. J. Anaesth.* 2015, 115 (1), 112-121.
6. Ouyang, W.; Wang, G.; Hemmings, H. C., Isoflurane and propofol inhibit voltage-gated sodium channels in isolated rat neurohypophysial nerve terminals. *Molecular Pharmacology* 2003, 64 (2), 373-381.
7. Quiroz-Padilla, M. F.; Guillazo-Blanch, G.; Sanchez, M. Y.; Dominguez-Sanchez, M. A.; Gomez, R. M., Effects of Excitotoxic Lesion with Inhaled Anesthetics on Nervous System Cells of Rodents. *Curr. Pharm. Design* 2018, 24 (1), 4-14.
8. Perouansky, M.; Hemmings, H. C., Neurotoxicity of General Anesthetics Cause for Concern? *Anesthesiology* 2009, 111 (6), 1365-1371.
9. Irifune, M.; Sato, T.; Nishikawa, T.; Masuyama, T.; Nomoto, M.; Fukuda, T.; Kawahara, M., Hyperlocomotion during recovery from isoflurane anesthesia is associated with increased dopamine turnover in the nucleus accumbens and striatum in mice. *Anesthesiology* 1997, 86 (2), 464-475.
10. Shichino, T.; Murakawa, M.; Adachi, T.; Nakao, S.; Shinomura, T.; Kurata, J.; Mori, K., Effects of isoflurane on in vivo release of acetylcholine in the rat cerebral cortex and striatum. *Acta Anaesthesiol. Scand.* 1997, 41 (10), 1335-1340.
11. Uhrig, L.; Dehaene, S.; Jarraya, B., Cerebral mechanisms of general anesthesia. *Ann. Fr. Anest. Reanim.* 2014, 33 (2), 72-82.
12. Nicoll, R. A.; Madison, D. V., GENERAL-ANESTHETICS HYPERPOLARIZE NEURONS IN THE VERTEBRATE CENTRAL NERVOUS-SYSTEM. *Science* 1982, 217 (4564), 1055-1057.
13. Hemmings, H. C.; Akabas, M. H.; Goldstein, P. A.; Trudell, J. R.; Orser, B. A.; Harrison, N. L., Emerging molecular mechanisms of general anesthetic action. *Trends Pharmacol. Sci.* 2005, 26 (10), 503-510.
14. Taylor, N. E.; Chemali, J. J.; Brown, E. N.; Solt, K., Activation of D1 Dopamine Receptors Induces Emergence from Isoflurane General Anesthesia. *Anesthesiology* 2013, 118 (1), 30-39.
15. Leung, L. S.; Luo, T.; Ma, J. Y.; Herrick, I., Brain areas that influence general anesthesia. *Prog. Neurobiol.* 2014, 122, 24-44.
16. Adachi, Y. U.; Yamada, S.; Satomoto, M.; Higuchi, H.; Watanabe, K.; Kazama, T.; Mimuro, S.; Sato, S., Isoflurane anesthesia inhibits clozapine- and risperidone-induced dopamine release and anesthesia-induced changes in dopamine metabolism was modified by fluoxetine in the rat striatum: An in vivo microdialysis study. *Neurochem. Int.* 2008, 52 (3), 384-391.
17. Adachi, Y. U.; Yamada, S.; Satomoto, M.; Higuchi, H.; Watanabe, K.; Kazama, T., Isoflurane anesthesia induces biphasic effect on dopamine release in the rat striatum. *Brain Res. Bull.* 2005, 67 (3), 176-181.
18. Monti, J. M.; Monti, D., The involvement of dopamine in the modulation of sleep and waking. *Sleep Medicine Reviews* 2007, 11 (2), 113-133.
19. Michelson, N. J.; Kozai, T. D. Y., Isoflurane and ketamine differentially influence spontaneous and evoked laminar electrophysiology in mouse V1. *J. Neurophysiol.* 2018, 120 (5), 2232-2245.
20. Brodnik, Z. D.; Espana, R. A., Dopamine uptake dynamics are preserved under isoflurane anesthesia. *Neuroscience Letters* 2015, 606, 129-134.
21. Sharott, A.; Magill, P. J.; Harnack, D.; Kupsch, A.; Meissner, W.; Brown, P., Dopamine depletion increases the power and coherence

- ence of beta-oscillations in the cerebral cortex and subthalamic nucleus of the awake rat. *Eur. J. Neurosci.* 2005, 21 (5), 1413-1422.
22. Galati, S.; Mazzone, P.; Fedele, E.; Pisani, A.; Peppe, A.; Pierantozzi, M.; Brusa, L.; Tropepi, D.; Moschella, V.; Raiteri, M.; Stanzione, P.; Bernardi, G.; Stefani, A., Biochemical and electrophysiological changes of substantia nigra pars reticulata driven by subthalamic stimulation in patients with Parkinson's disease. *Eur. J. Neurosci.* 2006, 23 (11), 2923-2928.
23. Tye, K. M.; Mirzabekov, J. J.; Warden, M. R.; Ferenczi, E. A.; Tsai, H. C.; Finkelstein, J.; Kim, S. Y.; Adhikari, A.; Thompson, K. R.; Andalman, A. S.; Gunaydin, L. A.; Witten, I. B.; Deisseroth, K., Dopamine neurons modulate neural encoding and expression of depression-related behaviour. *Nature* 2013, 493 (7433), 537-+.
24. Suo, H. R.; Wang, Z. H.; Dai, G. L.; Fu, J. Z.; Yin, J.; Chang, L. Q., Polyacrylonitrile Nerve Conduits With Inner Longitudinal Grooved Textures to Enhance Neuron Directional Outgrowth. *J. Microelectromech. Syst.* 2018, 27 (3), 457-463.
25. Bai, W. B.; Kuang, T. R.; Chitrakar, C.; Yang, R. G.; Li, S. L.; Zhu, D. H.; Chang, L. Q., Patchable micro/nanodevices interacting with skin. *Biosens. Bioelectron.* 2018, 122, 189-204.
26. Xiao, G. H.; Song, Y. L.; Zhang, Y.; Xing, Y.; Zhao, H. Y.; Xie, J. Y.; Xu, S. W.; Gao, F.; Wang, M. X.; Xing, G. G.; Cai, X. X., Microelectrode Arrays Modified with Nanocomposites for Monitoring Dopamine and Spike Firings under Deep Brain Stimulation in Rat Models of Parkinson's Disease. *ACS Sens.* 2019, 4 (8), 1992-2000.
27. Johnson, M. D.; Franklin, R. K.; Gibson, M. D.; Brown, R. B.; Kipke, D. R., Implantable microelectrode arrays for simultaneous electrophysiological and neurochemical recordings. *Journal of Neuroscience Methods* 2008, 174 (1), 62-70.
28. Disney, A. A.; McKinney, C.; Grissom, L.; Lu, X. K.; Reynolds, J. H., A multi-site array for combined local electrochemistry and electrophysiology in the non-human primate brain. *Journal of Neuroscience Methods* 2015, 255, 29-37.
29. Meyyappan, M., Nano biosensors for neurochemical monitoring. *Nano Converg.* 2015, 2, 6.
30. Moon, J. M.; Thapliyal, N.; Hussain, K. K.; Goyal, R. N.; Shim, Y. B., Conducting polymer-based electrochemical biosensors for neurotransmitters: A review. *Biosens. Bioelectron.* 2018, 102, 540-552.
31. Liu, C. B.; Zhao, Y.; Cai, X.; Xie, Y.; Wang, T. Y.; Cheng, D. L.; Li, L. Z.; Li, R. F.; Deng, Y. P.; Ding, H.; Lv, G. Q.; Zhao, G. L.; Liu, L.; Zou, G. S.; Feng, M. X.; Sun, Q. A.; Yin, L.; Sheng, X., A wireless, implantable optoelectrochemical probe for optogenetic stimulation and dopamine detection. *Microsystems & Nanoengineering* 2020, 6 (1), 12.
32. He, E. H.; Xu, S. W.; Xiao, G. H.; Dai, Y. C.; Li, X. R.; Song, Y. L.; Gao, F.; Zhang, Y.; Xu, S. H.; Cai, X. X., MWCNTs/PEDOT:PSS nanocomposites-modified microelectrode array for spatial dynamics recording of epileptic discharges in multi-subregion of hippocampal slice. *Sens. Actuator B-Chem.* 2021, 329, 9.
33. Wang, K.; Tian, L.; Wang, T. H.; Zhang, Z. Q.; Gao, X. J.; Wu, L.; Fu, B.; Liu, X. H., Electrodeposition of alginate with PEDOT/PSS coated MWCNTs to make an interpenetrating conducting hydrogel for neural interface. *Compos. Interfaces* 2019, 26 (1), 27-40.
34. Donahue, M. J.; Sanchez-Sanchez, A.; Inal, S.; Qu, J.; Owens, R. M.; Mecerreyes, D.; Malliaras, G. G.; Martin, D. C., Tailoring PEDOT properties for applications in bioelectronics. *Materials Science & Engineering R-Reports* 2020, 140, 22.
35. Zhang, S.; Song, Y.; Wang, M.; Zhang, Z.; Fan, X.; Song, X.; Zhuang, P.; Yue, F.; Chan, P.; Cai, X., A silicon based implantable microelectrode array for electrophysiological and dopamine recording from cortex to striatum in the non-human primate brain. *Biosens Bioelectron.* 2016, 85, 53-61.
36. Stanley, G.; Gokce, O.; Malenka, R. C.; Südhof, T.; Quake, S. R., Continuous and Discrete Neuron Types of the Adult Murine Striatum. 2020.
37. Al - Muhtasib, N.; For Ce Lli, P. A.; Vicini, S., Differential electrophysiological properties of D1 and D2 spiny projection neurons in the mouse nucleus accumbens core. *Physiological Reports* 2018, 6 (13).
38. Homayoun, H.; Moghaddam, B., NMDA receptor hypofunction produces opposite effects on prefrontal cortex Interneurons and pyramidal neurons. *J. Neurosci.* 2007, 27 (43), 11496-11500.
39. Dai, Y. C.; Song, Y. L.; Xie, J. Y.; Xiao, G. H.; Li, X. Y.; Li, Z. Y.; Gao, F.; Zhang, Y.; He, E. H.; Xu, S. W.; Wang, Y.; Zheng, W. F.; Jiang, X. Y.; Qi, Z. M.; Meng, D. D.; Fan, Z. W.; Cai, X. X., CB1-Antibody Modified Liposomes for Targeted Modulation of Epileptiform Activities Synchronously Detected by Microelectrode Arrays. *ACS Applied Materials & Interfaces* 2020, 12 (37), 41148-41156.
40. Csicsvari, J.; Hirase, H.; Czurko, A.; Buzsaki, G., Reliability and state dependence of pyramidal cell-interneuron synapses in the hippocampus: an ensemble approach in the behaving rat. *Neuron* 1998, 21 (1), 179-189.
41. Buzsaki, G.; Anastassiou, C. A.; Koch, C., The origin of extracellular fields and currents - EEG, ECoG, LFP and spikes. *Nat. Rev. Neurosci.* 2012, 13 (6), 407-420.
42. Gokce, O.; Stanley, G. M.; Treutlein, B.; Neff, N. F.; Camp, J. G.; Malenka, R. C.; Rothwell, P. E.; Fuccillo, M. V.; Südhof, T. C.; Quake, S. R., Cellular Taxonomy of the Mouse Striatum as Revealed by Single-Cell RNA-Seq. *Cell Reports* 2016, 16 (4), 1126-1137.
43. Krasowski, M. D.; Harrison, N. L., General anaesthetic actions on ligand-gated ion channels. *Cell. Mol. Life Sci.* 1999, 55 (10), 1278-1303.
44. Henneman, E. A.; Karras, G. E., Determining brain death in adults: a guideline for use in critical care. *Mercy Medical Center, Springfield, Mass. Critical Care Nurse* 2004, 24 (5), 50-52.
45. Wijdicks, E. F. M., DETERMINING BRAIN-DEATH IN ADULTS. *Neurology* 1995, 45 (5), 1003-1011.
46. Stratmann, G.; Sall, J. W.; May, L. D. V.; Bell, J. S.; Magnusson, K. R.; Rau, V.; Visrodia, K. H.; Alvi, R. S.; Ku, B.; Lee, M. T.; Dai, R., Isoflurane Differentially Affects Neurogenesis and Long-term Neurocognitive Function in 60-day-old and 7-day-old Rats. *Anesthesiology* 2009, 110 (4), 834-848.
47. Noguchi, K. K.; Johnson, S. A.; Dissen, G. A.; Martin, L. D.; Manzella, F. M.; Schenning, K. J.; Olney, J. W.; Brambrink, A. M., Isoflurane exposure for three hours triggers apoptotic cell death in neonatal macaque brain. *Br. J. Anaesth.* 2017, 119 (3), 524-531.
48. Brambrink, A. M.; Evers, A. S.; Avidan, M. S.; Farber, N. B.; Greeley, C. E.; Olney, J. W., Isoflurane-induced Neuroapoptosis in the Neonatal Rhesus Macaque Brain: Isoflurane or Ischemia-Reperfusion? Reply. *Anesthesiology* 2010, 113 (5), 1245-1246.

